Effect of the Soluble Block Size on Spherical Diblock Copolymer Micelles

Isaac LaRue,[†] Mireille Adam,[†] Ekaterina B. Zhulina,[‡] Michael Rubinstein,[†] Marinos Pitsikalis,[§] Nikos Hadjichristidis,[§] Dimitri A. Ivanov,[||] Raluca I. Gearba,[||,⊥] Denis V. Anokhin,[||] and Sergei S. Sheiko*,[†]

Department of Chemistry, University of North Carolina at Chapel Hill, Chapel Hill, North Carolina 27599-3290; Institute of Macromolecular Compounds of the Russian Academy of Sciences, 199004 St. Petersburg, Russia; Department of Chemistry, University of Athens, Panepistimiopolis, Zografou, 157 71 Athens, Greece; and Institut de Chimie des Surfaces et Interfaces, CNRS UPR 9069, 15 rue Jean Starcky, 68057 Mulhouse, France

Received February 22, 2008; Revised Manuscript Received June 25, 2008

ABSTRACT: While the effect of the insoluble block length on micelle properties is well understood, the effect of the soluble block is still controversial. We, therefore, have investigated the effect of the molecular weight of the soluble block on the critical micelle concentration (CMC), aggregation number, and hydrodynamic radius of spherical polymer micelles. Spherical micelles were formed from polystyrene-*b*-polyisoprene (PS-*b*-PI) in heptane, which was a good solvent for PI and a poor solvent for PS. Measurements were performed on two series of PS-*b*-PI with a constant PS block (19 and 39 kDa, respectively) and PI blocks varying from 10 to 100 kDa. For samples with large PI blocks, the experimental data were found to be in agreement with the commonly used star-like model. However, the experimental data for samples with short PI blocks deviated from the crew-cut micelle model. To correctly capture the crossover between the crew-cut and star-like regimes, it was found necessary to use recently developed scaling theory which explicitly considers all contributions to the free energy of the micelle. In agreement with theory, the aggregation number decreased while hydrodynamic radius and CMC increased with the molecular weight of the PI block. An interesting finding of these experiments is that the micelles of the 19 kDa series are in equilibrium at 25 °C, whereas the 39 kDa samples with the longer PS core block are "frozen" at room temperature. This was confirmed by SAXS measurements of core expansion upon heating which revealed a glass transition temperature of the 39 kDa samples at 28 ± 1 °C. The temperature value is consistent with 10% swelling of the PS core with heptane as determined by SAXS and SLS.

Introduction

When diblock polymers are dissolved in a selective solvent (good solvent for one block and poor solvent for the other) above a certain concentration, called the critical micelle concentration (CMC), the diblocks will associate to form micelles with a core of the insoluble block and a corona of the soluble block.[1−4] The free energy of the micelle is the sum of the free energies of the core, corona, and interface between them. By forming micelles, the diblocks are able to lower their free energy, since the insoluble blocks aggregate and thus reduce their interface with the solvent. However, formation of micelles results in extension of the core and corona blocks raising their elastic free energy. As a result, changing the size of the two blocks changes the balance of the free energy and in turn changes the aggregation number, the micelle hydrodynamic radius, and the CMC.

There has been a significant amount of work on the micelles structure for different types of neutral[5−11] and charged[12−14] block copolymers. Since molecular weight of the insoluble block has a stronger effect on the micellar properties than the soluble block does, most of these studies have focused on the effect of the insoluble core-block weight. The few that did investigate the effect of the soluble block used complicated systems containing charged blocks or solvent mixtures, both of which are difficult to compare with currently available theories.

To understand the effect of the soluble block, we have done a systematic study on PS-*b*-PI micelles in *n*-heptane (selective solvent for polyisoprene) as a function of the molecular weight of the PI block. We studied two series of PS-*b*-PI diblocks with a constant PS block (19 and 39 kDa, respectively) and PI blocks varying from 10 to 100 kDa. The experimental data were compared with two asymptotic theories based on the star-like and crew-cut micelle models[4,15−17] as well as with the recently developed scaling theory describing the crossover behavior between the two asymptotes.[18] Unlike the star-like and crew-cut asymptotic models, which neglect the contribution of the micelle core, the new scaling theory explicitly includes all three contributions into the free energy (core, corona, and their interface) and thus becomes applicable in a broader range of the block lengths. The star-like model, which considers the balance of the free energy between the star-like corona and the surface energy, was found to be valid for large soluble block size, where the contribution of the insoluble block is minor. However, as the PI block length was decreased, the star-like model began to deviate significantly from the experimental data. When the thickness of the soluble corona is small, compared to the radius of the insoluble core, the properties of polymer micelles are usually described by the crew-cut model, which considers the free energy balance of the planar corona and surface energy. However, the predictions of the crew-cut model were found to deviate from our experimental data, even for very short PI blocks, where one would expect the model to be valid. When the experimental data are compared with the new scaling theory,[18] we find excellent agreement with theory for the aggregation number and hydrodynamic radius for both series in the whole range of PI block size.

* Corresponding author. E-mail: Sergei@email.unc.edu.
[†] University of North Carolina at Chapel Hill.
[‡] Russian Academy of Sciences.
[§] University of Athens.
[||] CNRS UPR 9069.
[⊥] Present address: Brookhaven National Laboratory, National Synchrotron Light Source, 75 Brookhaven Avenue, Upton, NY 11973.

10.1021/ma800403r CCC: $40.75
Published on Web 08/08/2008

The likely vitrification of the polystyrene (bulk glass transition temperature $T_g \simeq 105$ °C) in micelle core raises the question of equilibration which is one of the most vital issues when studying polymer micelles.[19−21] To this end, much work has been done to study the micellization kinetics.[22−26] While these studies have provided a wealth of information, the kinetics of micellization appears to be very dependent on specifics of the studied systems. As will be discussed later in this paper, we have found that even within the same system (i.e., PS-*b*-PI diblocks in *n*-heptane) micelles formed with 19 kDa PS core block are in equilibrium at room temperature, while those formed from 39 kDa PS block are only in equilibrium at elevated temperatures ranging from ca. 30 to 50 °C.

Experimental Section

Materials. Two series of polymer samples were used; each had a fixed length of the PS block (either 19 or 39 kDa) and different molecular weight of PI blocks ranging from 10 to 100 kDa (Table 1). The 39 kDa series was purchased from Polymer Standards Service. The second series with 19 kDa PS blocks was synthesized by anionic polymerization high-vacuum techniques.[27] Styrene was polymerized in benzene at room temperature using *sec*-BuLi as initiator. A small quantity of the living PS−Li solution was sampled for characterization, and the rest was divided to calibrated cylinders, which were removed from the polymerization apparatus by heat sealing. The PS−Li content of each cylinder was used to initiate the polymerization of a predetermined amount of isoprene in separate polymerization apparatuses in order to prepare PS-*b*-PI block copolymers with the desired molecular weight of the PI block. The copolymers were precipitated in methanol and fractionated in toluene/methanol as the solvent/nonsolvent system in order to remove traces of deactivated PS block during the synthesis. The purified copolymers were precipitated in methanol and dried under vacuum.

Constitution, chemical composition, and molecular weight distribution of the prepared polymers were characterized by ^{1}H NMR, size exclusion chromatography (SEC), and low angle laser light scattering (LALLS). The measured molecular characteristics of the 19 kDa series are provided in the Supporting Information (Table S1). SEC experiments were conducted at 40 °C using a modular instrument consisting of a Waters model 510 pump, a Waters model U6K sample injector, a Waters model 401 differential refractometer, a Waters model 486 UV spectrophotometer, and a set of 4 m Styragel columns with a continuous porosity range from 10^6 to 10^3 Å. The columns were housed in an oven thermostated at 40 °C. THF was the carrier solvent at a flow rate of 1 mL/min.

The LALLS measurements were performed with a Chromatix KMX-6 low angle laser light scattering photometer at 25 °C equipped with a 2 mW He−Ne laser operating at $\lambda = 633$ nm. The concentration dependence of the reduced intensity is give by the following equation:

$$Kc/R_\theta = 1/M_w + 2A_2c + ... \quad (1)$$

where R_θ is the excess Rayleigh ratio of the solution over that of the solvent and K is the optical constant $K = [(4\pi^2n^2)/(\lambda^4 N_{Av})](dn/dc)^2$ using the refractive index of the solvent ($n = 1.405$), the wavelength of light ($\lambda = 633$ nm), Avogadro's number N_{Av}, and dn/dc is the refractive index increment (Supporting Information S1). Stock solutions were diluted with solvent to obtain appropriate concentrations. Refractive index increments, dn/dc, at 25 °C were measured with a Chromatix KMX-16 refractometer operating at 633 nm and calibrated with aqueous NaCl solutions.

The purity of the samples (i.e., lack of homopolymers) was verified by dynamic light scattering. The procedure of this test is described in the Supporting Information of a previous paper.[28] All solvents used for the micelle characterization were purchased from Fisher Chemicals or Acros Organics and were filtered through 0.2 μm NALGENE PTFE filters to remove any dust particles, prior to use.

Sample Preparation. Using filtered solvent, all diblock solutions were prepared by weighing. After being placed under argon, the samples were equilibrated at 60 °C for ~24 h and then slowly cooled to room temperature (~0.1 °C/min). The resulting solution was equilibrated at room temperature for at least 24 h prior to measurements.

Methods. Static light scattering measurements were done using a Brookhaven goniometer equipped with a Coherent argon laser using the 514 nm line, an operating power of 20−100mW, and a q range of 0.006−0.03 nm^{-1} ($q = (4\pi n/\lambda) \sin\theta$, where n is the refractive index of the solution, 2θ is the scattering angle, and $\lambda = 514$ nm is the wavelength). Light scattering measurements were preformed with a concentration range from 10^{-7} to 10^{-3}g/mL. Molecular weights were determined using the classical Zimm plot method.

Dynamic light scattering measurements were conducted using a BI-200SM light scattering system equipped with a "TurboCorr" digital correlator for signal processing. Autocorrelation functions were measured at three angles (60°, 90°, 120°) sample. The diffusion coefficient (D) was calculated by fitting the correlation curve to a single-exponential function for each angle (Supporting Information S3). The hydrodynamic radius (R_h) was then calculated from the diffusion coefficient of a spherical particle in a viscous liquid using the Stokes−Einstein equation, $D = kT/6\pi\eta R_h$, where k is the Boltzmann constant, T is the temperature, and η is the solvent viscosity. R_h was then determined by a single-exponential fit of the correlation function for each angle. The presented R_h values are an average of all three angles.

X-ray diffraction experiments were performed on the X33 camera of the European Molecular Biology Laboratory at the storage ring DORIS III of the Deutsches Elektronen Synchrotron DESY (Hamburg, Germany) and on the BM26 beamline of the E.S.R.F (Grenoble, France). In Hamburg the diffraction patterns were

Table 1. Characterization of PS-*b*-PI Micelles

	M_{PS}[a]	M_{PI}[b]	N_B[c]	N_A[d]	Q[e]	CMC,[f] g/mL	R_h,[g] nm	dn/dc,[h] mL/g
				39 kDa Series				
39-94	40 900	98 100	393	1443	120 ± 5	7.2×10^{-7}	54.2 ± 0.5	0.170
39-52	40 900	54 200	393	797	149 ± 7	3.2×10^{-7}	44.7 ± 0.2	0.178
39-26	40 900	28 000	393	412	292 ± 8	2.2×10^{-7} [i]	36.3 ± 0.3	0.188
39-15	40 900	16 600	393	244	410 ± 11	1.5×10^{-8} [i]	31.9 ± 0.6	0.195
				19 kDa Series				
19-99	19 400	98 600	187	1450	31 ± 1	5.7×10^{-5}	38.6 ± 0.3	0.161
19-59	19 400	58 700	187	863	51 ± 2	2.2×10^{-5}	31.6 ± 0.2	0.167
19-26	19 400	25 900	187	381	107 ± 3	3.1×10^{-6}	23.4 ± 0.3	0.178
19-19	19 400	19 200	187	282	128 ± 10	1.9×10^{-6}	20.2 ± 0.3	0.183
19-14	19 400	13 600	187	200	161 ± 2	3.3×10^{-6}	19.9 ± 0.7	0.188

[a] Weight-average molecular weight of the polystyrene block. [b] Weight-average molecular weight of the polyisoprene block. [c] Degree of polymerization of the insoluble polysterene block. [d] Degree of polymerization of the soluble polyisoprene block. [e] Aggregation number of PS-*b*-PI micelles at 25 °C in *n*-heptane. [f] Critical micelle concentration at 25 °C in *n*-heptane. [g] Hydrodynamic radius at 25 °C in *n*-heptane. [h] Refractive index increment. [i] Samples 39-15 and 39-26 had very low CMC's, and it was only possible to measure the initial decrease in the aggregation number. In this case, we report CMC values obtained by extrapolation of the concentration dependence of aggregation number to $Q = 1$.

collected with a MAR345 image plate system. The wavelength of 1.5 Å and the sample-to-detector distance of 3.3 m define the accessible q range from 0.50 to 13.82 nm^{-1}. The samples were placed in a 100 μL flat liquid cell having mica windows. The q axis was calibrated using silver behenate. In Grenoble, the 2D diffraction patterns were acquired using a SAXS detector positioned at the end of a vacuum path ~1.5 m away from the sample. The sample temperature was controlled with a Linkam heating stage. The intensity of the X-ray scattering from a suspension of micelles is given by

$$I(q) = NP(q)\,S(q) \tag{2}$$

where N is the number of micelles in the irradiated volume, S is the structure factor describing the arrangement of micelles in space, and P is the form factor of a single micelle. For diluted micellar suspensions used in the present work, the values of $S(q) \sim 1$. The form factor of a sphere of radius R ($P(q,R)$) is given by the classical expression[29]

$$P(q,R) = C\left[V \times 3\frac{\sin(qR) - qR\cos(qR)}{(qR)^3}\right]^2 \tag{3}$$

In eq 3, V stands for the sphere volume and C is a constant. The form factor of a sphere is an oscillating function, which decays with q according to the Porod law. The first minimum of $P(q,R)$ is at $qR \sim 4.49$. In the case of a system of polydisperse spheres, the ripples due to the form factor of each sharp fraction of spheres become smeared. The scattering intensity in this case can be described as

$$I(q) = A_0\int_0^\infty P(q,R)\,G(R,R_0,\sigma)\,\mathrm{d}R \tag{4}$$

where A_0 is a constant and G is a size distribution function centered on R_0 and having a width σ. In the data analysis, the normalized Gaussian functions were chosen to represent the size distribution of micelles. The background correction was performed by taking into account the scattering of a pure solvent ($I_{sol}(q)$) measured in the same conditions and a constant background (A_2):

$$I(q) = \int_0^\infty P(q,R)\,G(R,R_0,\sigma)\,\mathrm{d}R + A_1 I_{sol}(q) + A_2 \tag{5}$$

The fits to the experimental data were carried out using the Marquardt−Levenberg algorithm[30]by minimizing the χ^2 function conventionally defined as

$$\chi^2 = \sum\left(\frac{y - y_i}{\sigma_i}\right)^2 \tag{6}$$

The batch-processing of the scattering curves was performed with purpose-built routines written in IGOR PRO (Wavemetrics Ltd.).

Sample morphology was confirmed visually through AFM measurements (Multimode, Nanoscope IIIa) by spin-casting the samples onto freshly cleaved mica and then scanning with soft Si probes (spring constant 5 N/m). As seen in Figure 1, the polymer samples form uniform spherical micelles.

Results and Discussion

When studying spherical polymer micelles, there are several parameters which characterize the micelle morphology. The most commonly studied parameters include the aggregation number (Q) and the hydrodynamic radius (R_h). In addition, it is possible to measure the core size (R_c), which gives the polymer fraction in the core as $\phi = 3QM_c/4\pi\rho N_{Av}R_c^3$, where M_c is the mass of the core block, ρ is the mass density of bulk polystyrene, and N_{Av} is the Avogadro number. Below we separately discuss three issues: (i) critical micelle concentration, (ii) the effect of the soluble block on the micelle morphology, and (iii) equilibration of the micelles with the glassy polystyrene core. In addition to Q, R_h, and R_c, one can find radii of gyration and second virial coefficients in the Supporting Information S5 (Table S2).

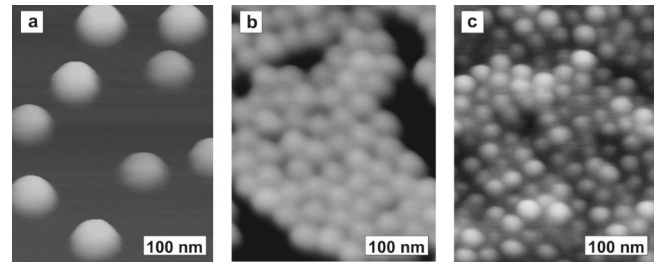

Figure 1. AFM height images of PS-*b*-PI spherical micelles formed from (a) sample 39−94 (R_h = 54 nm), (b) sample 39−15 (R_h = 32 nm), and (c) sample 19−14 (R_h = 20 nm). The micelles reduce in size upon decreasing the length of the soluble polyisoprene (PI) block (a, b) as well as the length of the insoluble polystyrene (PS) block (b, c). Cross-sectional profile analysis of the AFM images gives the following lateral and height dimensions of the micelles, respectively: $D = 70 \pm 5$ nm, $h = 13 \pm 1$ nm (sample 39-94), $D = 42 \pm 3$ nm, $h = 32 \pm 2$ nm (sample 39-15), $D = 35 \pm 2$ nm, $h = 12 \pm 1$ nm (sample 19-14).

I. Critical Micelle Concentration

CMC Measurements. Unlike low-molecular-weight surfactants, which have a sharp transition from unimer to micelles (Supporting Information S2), polymer micelles form over a broad concentration range. This effect has been explained by polydispersity of the blocks and is believed to be largely controlled by the polydispersity of the insoluble block.[31,32] Longer insoluble blocks provide stronger drive for the diblock to form micelles and thus result in lower CMC's.[33,34] Therefore, in the CMC region diblocks with longer insoluble blocks have started to form micelles while those with shorter insoluble blocks remain as unimers in solution. In a similar fashion, the CMC is also affected by the size of the soluble block. The CMC should decrease as the PI block is reduced because molecules with smaller soluble blocks carry lower "free energy cost" for being transferred from the unimer state to micellar corona. Here we show that the soluble block plays a significant role in determining the CMC value and thus broadening of the CMC region.

Since, in the CMC region, the aggregation number changes with concentration as diblocks begin to form micelles, it is impossible to extrapolate the scattering intensity to zero concentration as is necessary in the standard Zimm analysis. Thus, only an apparent aggregation number was measured as $Q_{app} \simeq M_w/M_0 \simeq R_\theta/KcM_0$ at a given concentration c, where M_0 is a block copolymer molecular weight and $M_w \simeq R_\theta/Kc$ is the weight-average micelle weight. For concentrations smaller than overlap concentration ($c \ll c^*$), this approximation is fairly accurate as seen from eq 1, which can be rewritten as $Kc/R_\theta \simeq 1/M_w + 2A_2c \simeq 1/M_w(1 + c/c^*)$. Here, the second virial coefficient and the overlap concentration are calculated as $A_2 \simeq N_AV/M^2 \simeq 1/Mc^*$ and $c^* = M/VN_A$, respectively.[33] Therefore, in the CMC range ($c \ll c^*$), one can use $Kc/R_\theta \simeq 1/M_w$ to calculate the apparent aggregation number $Q_{app} \simeq M_w/M_0$. Figure 2 shows a typical variation in the apparent aggregation number with concentration which was used to determine the CMC. Here we use the classical definition of the CMC: the concentration at which micelles are first detected; i.e., the measured aggregation number becomes larger than one ($Q > 1$). Table 1 demonstrates the strong effect the molecular weight of the PI block on the CMC. Decreasing the PI molecular weight by 1 order of magnitude causes the CMC to decrease by almost 2 orders of magnitude for both the 19 and 39 kDa series.

Temperature Dependence of the CMC. Since the decrease in the interfacial energy due to micellization is balanced by the

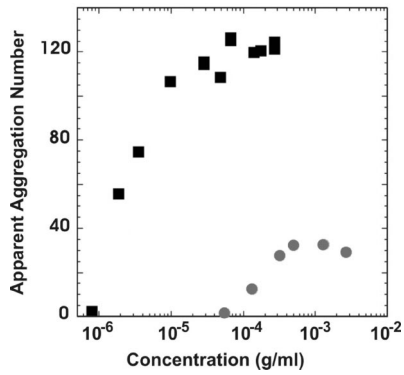

Figure 2. Plot of the apparent aggregation number vs concentration for PS-*b*-PI 39-94 (black squares) and 19-99 (gray circles) measured at 25 °C in *n*-heptane.

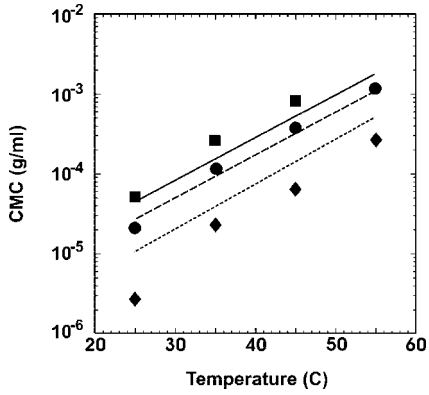

Figure 3. Plot of the variation of the CMC with temperature for samples 19-26 (diamonds), 19-59 (circles), and 19-99 (squares). Theoretical calculations for PI blocks with molecular weights of 26, 59, and 99 kDa are shown respectively by the dotted, dashed, and solid lines.

decrease in entropy, greater concentrations are needed before the unimer will start to aggregate and form micelles at higher temperatures. This results in the CMC increasing with temperature. We have studied the variation of the CMC with temperature for three samples of the 19 kDa series. As seen in Figure 3, when the temperature is changed from 25 to 55 °C, the CMC changes by almost 2 orders of magnitude. This is in good agreement with the CMC variations predicted by theory as shown by the lines in Figure 3 (see Appendix 1 for the corresponding equations). The observed discrepancy between theory and experiment in Figure 3 (especially for sample 19-26) is attributed to exponential sensitivity (eq A1, Appendix 1) of CMC measurements to small variations in temperature and diblock composition. Nevertheless, the agreement is regarded as good because the discrepancy remains within the same order of magnitude.

II. Morphology

Aggregation Number. Above the CMC, aggregation number of micelles increases with concentration and then levels off (Figure 2). In the plateau region, the equilibrium aggregation number Q can be measured using the standard Zimm plot analysis at low concentrations (Supporting Information S4). Theory predicts that the aggregation number should increase as the size of the soluble block is decreased.[18] Figure 4 demonstrates an excellent agreement between experiment and the new scaling theory (solid lines). In comparison, the asymptotic models of star-like (dashed lines) or crew-cut (dotted lines) micelles that are often used for calculating micelle parameters demonstrate poor agreement. The star-like model

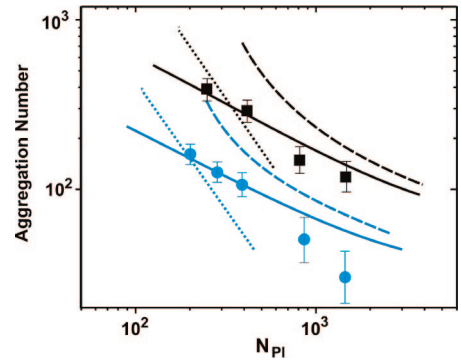

Figure 4. Log−log plots of the variation in the aggregation number with the degree of polymerization of the PI blocks. Black and blue symbols are for 39 and 19 kDa PS blocks respectively. The solid, dashed, and dotted lines are respectively the new crossover scaling solution, asymptotic star-like, and asymptotic crew-cut dependences.

becomes relevant when the corona thickness (H) grows to be larger than the core radius (R_c). In this range, the aggregation number is predicted[14] to scale with the degree of polymerization of the soluble block N_A as $Q \sim (1/\ln(N_A))^{6/5}$ (eq A9 in Appendix 1). For crew cut micelles ($R_c < H$), the aggregation number is predicted to depend more strongly on N_A as $Q \sim (1/N_A)^{3/2}$ (eq A14 in Appendix 1). As seen in Figure 4 at $N_A \equiv N_{PI} < 500$, the star-like approximation overestimates all of the aggregation numbers beyond the error bar but approaches the experimental data for the 39 kDa series at high PI molecular weight. This makes sense because the asymptotic star-like model ignores the core contribution, the relative role of which diminishes with the length of the soluble block. In contrast to the star-like model, the crew-cut model (dotted lines) predicts a much stronger dependence than is experimentally measured for all soluble blocks including the smallest ones (where it is expected to be most applicable). However, it is interesting that for longer soluble blocks of the 19 kDa series (two last points in Figure 4) the star-like asymptote as well as the new scaling theory do not appear to be as good of a fit, even though these samples are more star-like than the 39 kDa. This is explained by the noticeably higher CMC values of the high-molecular-weight 19 kDa samples (Supporting Information S4), resulting in a narrower concentration range between the CMC and the overlap concentration (where one usually determines the aggregation number). This makes the Zimm analysis less accurate due to the need to extrapolate the data to zero concentration. Therefore, we used the lowest Kc/R values for determination of the aggregation numbers.

Hydrodynamic Radius. The total radius of a micelle is the sum of two sizes: the radius of the core (R) and the thickness of the corona (H), i.e. $R_{total} = R + H$. Theory predicts that the total radius increases with the degree of polymerization of the soluble block, while its individual components, i.e. R and H, exhibit opposite behaviors. While the corona thickness should increase with the degree of polymerization of the soluble block, the core radius is predicted to decrease. The latter prediction is consistent with the decrease of the aggregation number (Figure 4), assuming that the density inside the core remains constant.

Dynamic light scattering was used to determine the hydrodynamic radius (R_h) of our micelles. Here, it is important to emphasize that polymer micelles are not dense objects. Penetration of solvent through the polymer screens hydrodynamic interactions on the scale of the last (external) correlation blob of the corona. To take this into account, a

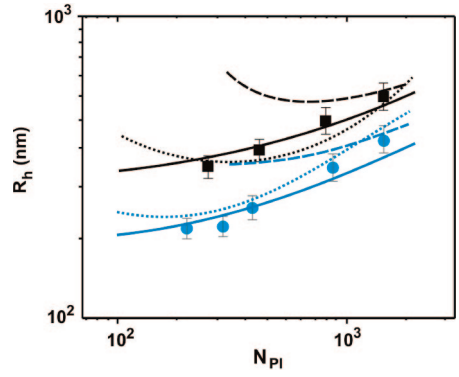

Figure 5. Log−log plots of the hydrodynamic radius as a function of PI degree of polymerization. Black and blue symbols are for 39 and 19 kDa PS blocks, respectively. The solid, dashed, and dotted lines are respectively the new crossover scaling solution, asymptotic star-like, and asymptotic crew-cut dependences.

small correction to the total radius resulting in R_h being calculated as

$$R_h = R_{total} - C\xi_{last} \quad (7)$$

where R_{total} is the sum of the core radius and corona thickness, C is a numerical coefficient on the order of unity, and $\xi_{last} = R_{total}/\sqrt{Q}$ is the size of the last corona blob.[18] As seen in Figure 5, the adjusted values from the crossover scaling model (solid lines) and the experimental data are in good agreement. The star-like asymptotes for R_h (dashed lines) overestimate the experimental data for short PI blocks but become close to the experimental data as the soluble block size increases. The crew-cut model (dotted lines) is found to correctly predict the magnitude of the values; however, it exhibits wrong trend as the size the soluble block decreases. Here it is important to emphasize that all experimental data in this paper, including the R_h values, for two series of nine different diblocks were described by the scaling model using a single set of only three fitting parameters C_F, C_H, and C. Both solid lines in Figure 5 were calculated using $C = 0.5$ (Table A1 in Appendix 1), which is consistent with the scaling assumption $C \sim 1$; i.e., the hydrodynamic penetration length is on the order of the last correlation blob in the corona (eq 7).

III. Micelle Equilibration

The glassy nature of the PS core raises an issue whether the studied PS-*b*-PI micelles are in equilibrium. Depending on the amount of solvent swelling the micelle core, the PS core, which has a bulk glass-transition temperature of $T_g = 105$ °C, can vitrify at different temperatures below 105 °C. In order to determine the glass-transition temperature and thus verify the equilibrium, two sets of experiments were conducted. First, we studied the temperature response of the aggregation number in the CMC range. Second, we measured the thermal expansion of the PS core by SAXS in solution at higher concentrations ($c > 10^{-3}$ g/mL) that are well above the CMC.

Temperature Variation of the Aggregation Number in the CMC Range. To study the temperature response, we used a procedure similar to Honda et al.,[22] except that we used temperature ramps instead of temperature jumps. The details of the equilibration procedure are outlined in Appendix 2. The CMC range was chosen because of much stronger response of the aggregation number to temperature variations in this concentration regime (Figure 3). When the temperature ramps were applied to the 19 kDa series, all of the samples were found to instantaneously and reversibly transform from micelles to unimers in the temperature range of 25−40 °C (Figure 6a). The

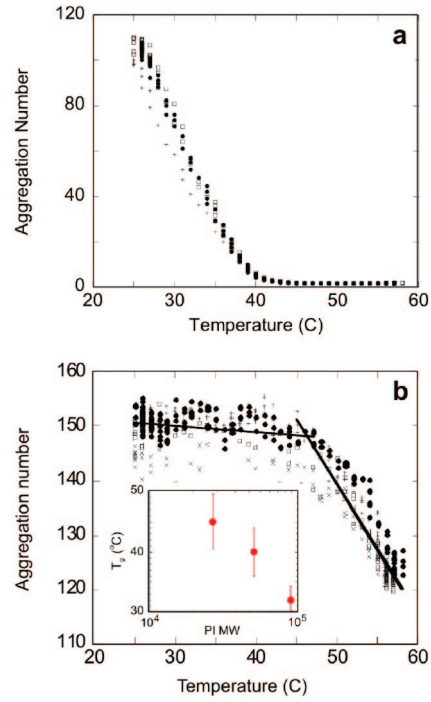

Figure 6. Variation in the aggregation number with temperature was measured for two samples, i.e., (a) 19−26 at a concentration of 6.2×10^{-5}g/mL and (b) 39−26 at a concentration of 3.7×10^{-6}g/mL. The multiple data points correspond to measurements taken during two subsequent heating−cooling cycles in range from 25 to 60 °C. Inset in (b): plot of the apparent T_g variation with PI molecular weight for the 39 kDa series.

prompt response indicates that the 19 kDa series is in equilibrium at 25 °C. When the same procedure was applied to the 39 kDa series, the onset of the micelle dissociation was observed at higher temperatures, e.g. at $T > 45$ °C for the 39−26 sample in Figure 6b. The hindered dissociation of the 39 kDa micelles suggests that the micelles have a glassy core and thus may be out of equilibrium at temperatures below 45 °C. One may ascribe the onset of micelle dissociation to glass transition of the PS core due to the plasticization effect of *n*-heptane which enters into the core lowering the core density along with its glass transition temperature (discussed below). An unusual feature of these data is that this apparent glass transition temperature of the PS core changes with the size of the soluble PI block (inset in Figure 6b). This contradicts the general presumption that the core density is largely controlled by polymer−solvent interactions within the core and should be almost independent of the size of the soluble block in the corona.

Core Density. In order to measure the core density of PS-*b*-PI micelles, we separately measured the aggregation number (Q) by light scattering (Figure 4 and Table 1) and the core radius (R_c) by small-angle X-ray scattering (SAXS). The polymer fraction in the core was calculated as $\phi = 3QM_c/4\pi\rho N_{Av}R_c^3$, where M_c is the mass of the core block and ρ is the mass density of bulk polystyrene. Figure 7 shows typical SAXS curves that were measured for two samples of the 39 kDa series. Data analysis was performed by fitting the curves with a model of polydisperse spheres, which neglects the contribution from the PI corona. It can be seen that the fits reproduce the main features of the curves such as the ripples due to the scattering from the electron-rich PS core. Table 2 depicts the values of the core radius and the corresponding core density for the two series of samples (39 and 19 kDa). Within the 10% experimental error, the volume fraction of polystyrene in the micelle core exhibits only weak (if any) dependence on the degree of polymerization of the soluble block. In contradiction to Figure 6, the obtained

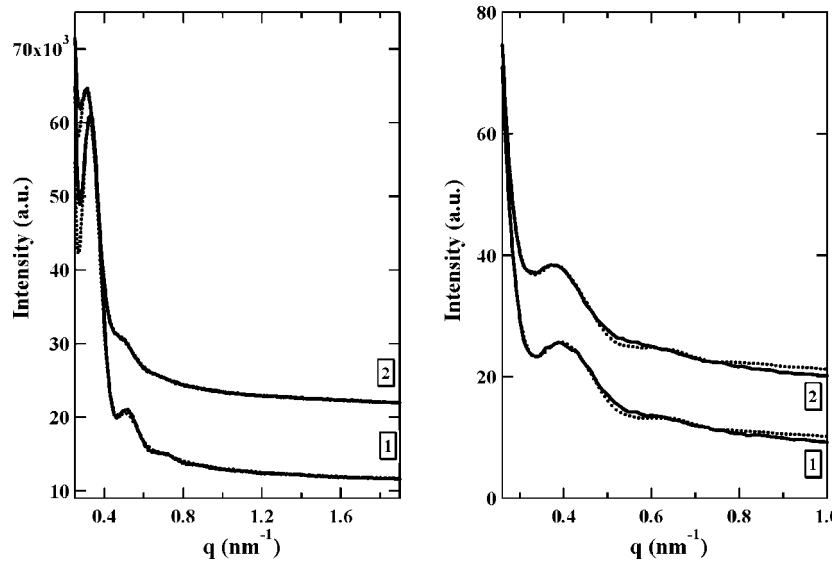

Figure 7. SAXS curves corresponding to PS block of 39K and PI block of 26K (left) and 52K (right) measured at two different temperatures: (1) 25 and (2) 70.4 °C. The fits with a model of polydisperse spheres are given in dotted lines. The curves are vertically offset for clarity.

Table 2. Core Density of PS-*b*-PI Micelles

sample	R_c,[a] nm	ϕ_{PS}[b]	α,[c] 10^4 K^{-1}
39-94	13.3	0.79 ± 0.06	6.6
39-52	13.7	0.89 ± 0.07	8.8
39-26	17.2	0.89 ± 0.08	7.9
19-99	6.0	1.05 ± 0.05	N/A[d]
19-59	7.0	1.10 ± 0.10	N/A[d]
19-26	9.1	1.06 ± 0.09	N/A[d]

[a] Radius of the PS core was measured by SAXS in *n*-heptane. [b] The volume fraction of polymer in the micelle core was calculated as $\phi = V_{PS}/V_{core} = (3/4\pi)(QM_{PS}/N_{Av}\rho R_c^3)$, where Q is the aggregation number measured by SLS in *n*-heptane and ρ = 1.05 g/cm^3 is the mass density of polystyrene. [c] The linear thermal expansion coefficient of the PS core was measured by SAXS in *n*-heptane in a range of 30−65 °C, i.e., above the glass transition temperature. [d] Not available due to large experimental error. The fits to the micelle suspension having the shortest PI block are less satisfactory in the low angle region, close to the position of the first ripple (Figure 7).

data indicate that all micelles have nearly the same fraction of heptane in the core and thus should have similar glass transition temperatures. This conclusion, however, needs to be verified by direct measurements of the core glass-transition temperature which is exhibits strong sensitivity to variations in the core density (Appendix 3).

***T_g* of the Micelle Core.** The glass transition temperature of the micelle core was determined from thermal expansion of the micelle core by temperature-dependent synchrotron X-ray scattering. The measurements were conducted at high concentrations, above the CMC but below the overlap concentration (CMC < c < c*), where the aggregation number weakly depends on temperature. As shown in Figure 8, the micelles of all three samples, i.e. 39-26, 39-53, and 39-93, clearly exhibit a similar glass transition temperature of about T_g = 28 °C. Here we should note that one has to be prudent when interpreting T_g measurements of microheterogeneous systems, such as block copolymer micelles, since various factors (size, shape, density distribution, and chemical composition) may affect their thermal properties. The observed similarity of T_g values merely indicate that different diblocks have similar structure of the polystyrene core. However, microscopic details of the core structure remain ambiguous.

At $T > T_g$, the size of the core for all three systems steadily increases with temperature. The rate of this increase can be characterized by a linear coefficient of thermal expansion ranging from 6.6 × 10^{-4} to 8.8 × 10^{-4} K^{-1}, which is close to

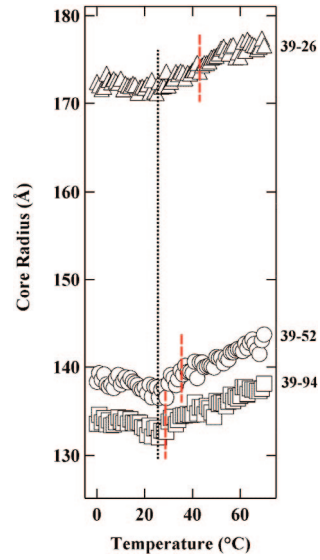

Figure 8. Variation of the core size as a function of temperature was measured for PS-*b*-PI micelles with PS block of 39K and PI block of 94K, 52K, and 26K by temperature-dependent small-angle X-ray scattering in *n*-heptane. The red dashed lines indicate the onset temperature of micelles dissociation in the CMC region (Figure 6b).

the corresponding bulk values and indicates that the PS core is in the rubbery state.[35]It is interesting to compare the T_g of the PS core to earlier reported effect of the T_g depression due to plasticization effect of heptane. For example, in studies of solvent-induced crazing of PS by Kambour et al.,[36] it was found that the equilibrium uptake of heptane by PS at ambient temperature equals ∼11.9% (w/w). The swelling of PS was accompanied by lowering of its T_g measured by DSC to −11 °C. However, the authors mentioned some difficulties in the calorimetric measurements on swollen films and the associated imprecisions. In a later publication, Krenz et al.[37] pointed out that the value of Kambour et al. might be underestimated and suggested a higher calorimetric T_g of 11 °C. In a similar work,[38] the T_g of swollen PS measured with a torsion pendulum is even higher (32.5 °C), but the temperatures cannot be directly compared to the DSC data given the influence of the measurement frequency. The T_g decrease due to the solvent uptake can be also estimated by the Fox equation assuming the efficient glass transition temperature of heptane to be −176 °C, as

computed from the data of Krenz et al. Figure 11 shows that the T_g values of 28 ± 1 °C should correspond to 8.5 ± 1.2 wt % of heptane in the PS core. Additional error in the heptane fraction is due to uncertainty in calculation of the glass transition temperature of heptane. The determined fraction of heptane in the micelle core is consistent with the measured polymer fraction of the 39 kDa series ranging from 0.79 ± 0.06 to 0.89 ± 0.08 (Table 2). Therefore, the temperature-dependent synchrotron SAXS measurements of the core size confirm weak dependence of both the core density and the glass transition temperature on the size of the PI block. The deviation of the T_g values from the dissociation-onset temperatures (dashed lines in Figure 8) is attributed to a broad distribution of core diameters in the CMC range, which may range from ca. 1 to 30 nm and result in significant variations of the glass transition temperature.

Conclusions

The critical micelle concentration (CMC), aggregation number (Q), and hydrodynamic radius (R_h) were measured as a function of polyisoprene (PI) molecular weight for two molecular weights of polystyrene (19 and 39 kDa) in the selective solvent heptane. The CMC and R_h were found to increase with PI molecular weight, while the aggregation number was found to decrease. Increasing the PI molecular weight by 1 order of magnitude causes the CMC to increase by almost 2 orders of magnitude. The R_h was found to have a weak dependence on the molecular weight of the PI block, increasing respectively by about 90 and 60% for the 19 and 39 kDa series when the PI molecular weight was increased from 10 to 100 kDa. The same variation in PI molecular weight causes the aggregation number to decrease by close to an order of magnitude for the 19 kDa series, while it has a weaker effect on the 39 kDa series. In the whole range of experimental data, we find excellent agreement between our data and recently developed scaling crossover theory for the aggregation number and hydrodynamic radius for both series. In contrast, theory for star-like polymer micelles was found to approach our experimental data only for high values of the polyisoprene molecular weight, while theory for crew-cut micelles deviated significantly from our experimental data (even at low molecular weight values, where it should be valid). In other words, diblocks with typical N_A and N_B values ranging from 100 to 1000 do not demonstrate clear "crew-cut" behavior prior their transition to cylindrical morphology. However, one may observe the "crew-cut" exponents for longer diblocks that are predicted to have a broader crew-cut range.[18] We also demonstrated that it was important to check for sample equilibration, as micelles with a PS core can freeze at different temperatures depending on the size of the blocks used. It was found that both the mass density and the glass transition temperature of the PS core appeared to be independent of the size of the soluble block (Figure 8); however, further experiments are needed to understand the effect of the size of the soluble block on the micelle dissociation onset temperature in CMC range (Figure 6).

Acknowledgment. We thank the National Science Foundation NIRT ECS0103307 for funding, and the STC Program of the National Science Foundation under Agreement CHE-9876674 for funding and shared facilities. E.B.Z. acknowledges financial support from the Russian Foundation for Basic Research (RFBR 05-3-33126). D.A.I. acknowledges financial support from the CNRS (France) ATIP project and from the European Community's 'Marie-Curie Actions' under Contract MRTN-CT-2004-504052 [POLYFILM]. R.I.G. is a postdoctoral researcher of the CNRS. We acknowledge the European Synchrotron Facility for provision of synchrotron radiation facilities. The synchrotron radiation work was supported by the European Union through the HCMP Access to Large Installation Project, Contract HPRI-CT-1999-00017 to the EMBL-Hamburg. We thank W. Bras, D. Svergun, and M. Roessle for assistance in synchrotron experiments.

Appendix 1. Equations

Here we present theoretical equations that were developed in ref 18 to calculate CMC and dimensions of PS-*b*-PI block copolymer micelles using star-like model, crew-cut model, and the new crossover theory. All numerical coefficients and other model parameters are presented in Table A1.

a. Critical Micelle Concentration. The CMC is calculated from the difference between the free energies of a block copolymer molecule in the micelle and unimer states:

$$\ln(c_{CMC}) \approx [F_3(Q) - F_{s0}]/kT \tag{A1}$$

Here, F_{30} is the surface energy of a unimer (eq 10 in ref 14) and $F_3(Q)$ is the free energy of a block copolymer chain in a spherical micelle (eq 13 in ref 14):

$$\frac{F_{s0}}{kT} = (36\pi)^{1/3}\gamma\left(\frac{N_B}{\phi}\right)^{2/3} \tag{A2}$$

$$\frac{F_3}{kT} = \frac{3\pi^2 r_3^{\,2}}{80 p_B N_B} + \gamma\frac{3N_B}{\phi r_3} + \frac{1}{2\sqrt{3}}C_F p_A^{\,-3/4}\frac{r_3^{\,3/2}\varphi^{1/2}}{N_B^{\,1/2}} \ln\left[1 + \frac{2C_H p_A^{\,1/4} N_A \varphi^{1/2} a_A^{\,2}}{\sqrt{3} r_3^{\,1/2} N_B^{\,1/2} a_B^{\,2}}\right] \tag{A3}$$

Using eq 2 for F_{s0}, one obtains

$$\ln(c_{CMC}) \approx F_3(Q)/kT - (36\pi)^{1/3}\gamma\left(\frac{N_B}{\varphi}\right)^{2/3} \tag{A4}$$

The temperature dependence of the surface energy is given by eq 59 in ref[14]

$$\gamma\varphi^{-2/3} = (0.14 \pm 0.002) - (1.07 \pm 0.04)\times 10^{-3}(T - 273) \tag{A5}$$

b. Dimensions of Block Copolymer Micelles. *Star-like Model*: Using the star-like model, the hydrodynamic radius of a diblock-copolymer micelle is calculated as follows:

$$R_h = R_{total} - C\xi_{last} = R_{total} - C\frac{R_{total}}{\sqrt{Q}} = R_{total}\left(1 - \frac{C}{\sqrt{Q}}\right) = (R_{3star} + H_{3star})\left(1 - \frac{C}{\sqrt{Q}}\right) \tag{A6}$$

R_{3star}, H_{3star}, and Q are the radius of the micelle core, thickness of the micelle corona, and the micelle aggregation number, respectively:

$$R_{3star} \approx a_B\left(\frac{N_B}{\varphi}\right)^{3/5}\left(\frac{4\sqrt{3}p_A^{\,3/4}}{C_F K}\gamma\right)^{2/5} \tag{A7}$$

$$H_{3star} \approx a_A N_A^{\,1/2}\left(\frac{4\sqrt{3}}{C_F K}\gamma\right)^{3/10}\left(\frac{N_B}{\varphi}\right)^{1/5} p_A^{\,7/20}\left(\frac{2C_H}{\sqrt{3}}\right)^{1/2} \tag{A8}$$

Table A1. Parameters That Were Used To Calculate the Lines in Figures 3−5 (See Also Table 2 in Ref 14 for More Details)

a_A[a]	a_B[a]	p_A[b]	p_B[b]	φ[c]	$\gamma/\varphi^{2/3}$[d]	C_F[e]	C_H[e]	C[e]
5.0 Å	5.6 Å	1.6	1.5	0.85	0.11	1.36	0.62	0.5

[a] a_A and a_B are monomers sizes of polyisoprene and polystyrene, respectively. [b] p_A and p_B are stiffness parameters (p = Kuhn length/monomer size) of polyisoprene and polystyrene, respectively. [c] Volume fraction of polystyrene in the micelle core measured by SAXS and SLS. [d] ψ is the surface free energy per monomer (per area a^2) in kT units as measured by SLS (see eq 59 of ref 14). [e] Numerical coefficients determined by fitting the predicted theoretical dependences with the experimental data for the micelles dimensions. The slightly different values compared to those in ref 14 are due to the newly and more accurately measured volume fraction φ = 0.85.

$$Q_{3\mathrm{star}} = \frac{4\pi\varphi}{3N_\mathrm{B}} r_{3\mathrm{star}}{}^3 \approx \frac{4\pi}{3}\left(\frac{4\sqrt{3}p_\mathrm{A}{}^{3/4}}{C_\mathrm{F}}\frac{\lambda}{K}\right)^{6/5}\left(\frac{N_\mathrm{B}}{\varphi}\right)^{4/5} \quad \text{(A9)}$$

where K is a logarithmic term denoted as

$$K = \ln\left(\frac{2C_\mathrm{H}p_A{}^{1/4}N_\mathrm{A}\varphi^{1/2}a_\mathrm{A}{}^2}{\sqrt{3}N_\mathrm{B}{}^{1/2}a_\mathrm{B}{}^2 r_{3\mathrm{star0}}{}^{1/2}}\right) \quad \text{(A10)}$$

All numerical coefficients and other model parameters are listed below in Table A1.

Crew-Cut Model: Similar equations are used to calculate the hydrodynamic radius of a crew-cut micelle:

$$R_\mathrm{h} = (R_{3\mathrm{cc}} + H_1)\left(1 - \frac{C}{\sqrt{Q}}\right) \quad \text{(A11)}$$

$$R_{3\mathrm{cc}} \approx \frac{3N_\mathrm{B}}{\varphi}\frac{a_\mathrm{B}{}^2}{a_\mathrm{A}}\left(\frac{\gamma p_\mathrm{A}{}^{1/2}}{C_\mathrm{F}C_\mathrm{H}N_\mathrm{A}}\right)^{1/2} \quad \text{(A12)}$$

$$H_1 = \frac{a_\mathrm{A}{}^2}{a_\mathrm{B}}C_\mathrm{H}N_\mathrm{A}p_\mathrm{A}{}^{1/2}\left(\frac{\varphi r_1}{N_\mathrm{B}}\right)^{1/2} \quad \text{(A13)}$$

$$Q_{\mathrm{cc}} = \frac{4\pi r^3\varphi}{3N_\mathrm{B}} \approx \frac{36\pi N_\mathrm{B}{}^2}{\varphi^2}\left(\frac{\gamma a_\mathrm{B}{}^2 p_\mathrm{A}{}^{1/2}}{C_\mathrm{F}C_\mathrm{H}a_\mathrm{A}{}^2 N_\mathrm{A}}\right)^{3/2} \quad \text{(A14)}$$

Appendix 2. Micelle Equilibration Procedure

In order to study whether or not our micelles are in equilibrium, we modified the procedure used by Honda et al.[22] To do this, we first measured the variation in the temperature inside the scattering cell as the temperature of the circulating water bath was changed. We then measure the change in the scattering intensity of *n*-heptane during the temperature ramps. As seen in Figure 9, the two curves are superimposable. This means that it is then possible to calculate the heptane scattering intensity as a function of temperature. The same procedure can be used to measure the variation in the scattering intensity of micelle solutions with temperature. It is then possible to get the apparent aggregation number by subtracting the solvent scattering intensity from the solution intensity, multiplying by the Raleigh ratio of toluene, and dividing by the sample concentration and optical constant K, where $K = (4\pi^2 n^2/\lambda^4 N_\mathrm{Av})(\mathrm{d}n/\mathrm{d}c)^2$ and n is the refractive index of the solvent (1.388), λ is the wavelength of light used (514 nm), N_Av is Avogadro's number, and $\mathrm{d}n/\mathrm{d}c$ is the specific change in refractive index for a polymer solvent pair, which can be calculated. As seen in Figure 10, the change in the apparent aggregation number and temperature with time are well correlated; i.e., as the temperature increases, the aggregation number decreases. By correlating the aggregation number and temperature at a given time, it is then possible to obtain the variation in the aggregation number with temperature.

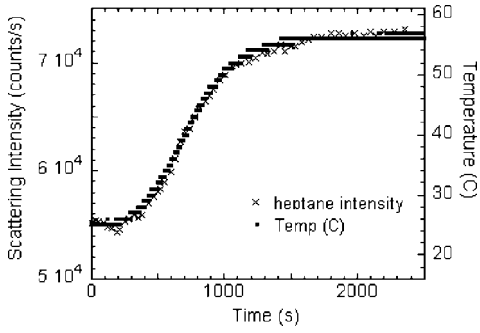

Figure 9. Double *Y* plot of the variation the scattering intensity of heptane measured at an angle of 20° and the temperature inside the scattering cell, measured during a different run, with time. As seen, the two are superimposable.

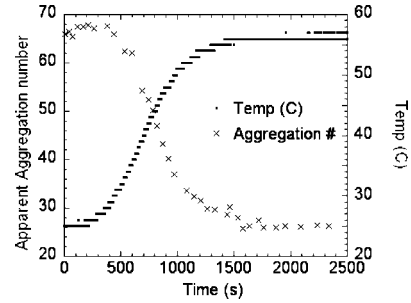

Figure 10. Plot of the change in the apparent aggregation number and temperature inside the scattering cell with time.

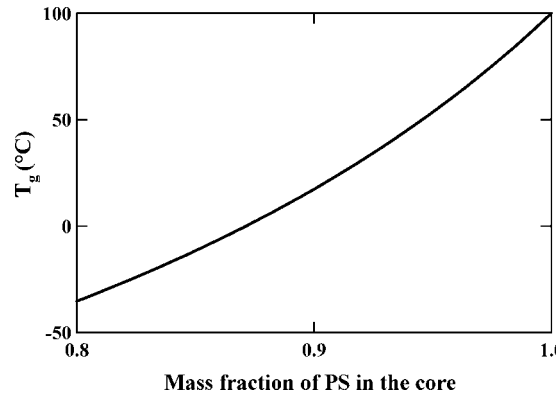

Figure 11. Glass transition temperature (T_g) of a PS/heptane system can be described by the Fox equation with a fictive T_g of heptane. The T_g values of about 30 °C correspond to ~8% of solvent in the core.

Appendix 3. Fox Equation

Figure 11 shows the decrease of the glass transition temperature of polystyrene due to swelling with *n*-heptane. The following Fox equation is used to calculate the glass transition:

$$T_\mathrm{g}{}^{-1} = \frac{w}{T_{\mathrm{g,PS}}} + \frac{1-w}{T_{\mathrm{g,heptane}}}$$

where w is the weight fraction of polystyrene (PS) and $(1 - w)$ the weight fraction of *n*-heptane. $T_{\mathrm{g,PS}} = 100$ °C is the glass transition temperature of atactic PS. For *n*-heptane, we used a fictive glass transition temperature of $T_{\mathrm{g,heptane}} = -176$ °C, which can be extracted from the data of Krenz et al.[28]

Supporting Information Available: Molecular characterization, evaluation of the CMC region width, representative correlation function in a dynamic light scattering experiment, and radii of gyration and second virial coefficients. This material is available free of charge via the Internet at http://pubs.acs.org.

References and Notes

(1) Tuzar, Z.; Kratochvil, P. *Surf. Colloid Sci.* **1993**, *15*, 1.
(2) Hamley, I. W. *The Physics of Block Copolymers*; Oxford Universtity Press: Oxford, England, 1998.
(3) Halperin, A.; Tirrell, M.; Lodge, T. P. *Adv. Polym. Sci.* **1992**, *100*, 31.
(4) Chocair, A.; Eisenberg, A. *Eur. Phys. J. E* **2003**, *10*, 37.
(5) Qin, A.; Tian, C.; Ramireddy, C.; Webber, S. E.; Munk, P.; Tuzar, Z. *Macromolecules* **1994**, *27*, 120.
(6) Khougaz, K.; Zhong, X. F.; Eisenberg, A. *Macromolecules.* **1996**, *29*, 3937.
(7) Förster, S.; Zisenis, M.; Wenz, E.; Antonietti, M. *J. Chem. Phys.* **1996**, *104*, 9956.
(8) Putaux, J. L.; Minatti, E.; Lefebvre, C.; Borsali, R.; Schappacher, M.; Deffieux, A. *Faraday Discuss.* **2005**, *128*, 163.
(9) Yan, X.; Liu, G.; Li, H. *Langmuir* **2004**, *20*, 4677.

(10) Bang, J.; Jain, S. M.; Li, Z. B.; Lodge, T. P.; Pedersen, J. S.; Skov Kesselman, E.; Talmon, Y. *Macromolecules* **2006**, *39*, 1199.
(11) Wang, X.; Guerin, G.; Wang, H.; Wang, Y.; Manners, I.; Winnik, M. A. *Science* **2007**, *317*, 644.
(12) Astafieva, I.; Khougaz, K.; Eisenberg, A. *Macromolecules* **1995**, *28*, 7127.
(13) Jacquin, M.; Muller, P.; Talingting-Pabalan, R.; Cottet, H.; Berret, J. F.; Futterer, T.; Theodoly, O. *Colloid Surf. Interface Sci.* **2007**, *316*, 897.
(14) Kaewsaiha, P.; Matsumoto, K.; Matsuoka, H. *Langmuir* **2007**, *23*, 9162.
(15) Halperin, A. *Macromolecules* **1987**, *20*, 2943.
(16) Zhulina, Y. B.; Birshtein, T. *Polym. Sci. USSR* **1985**, *27*, 511.
(17) Birshtein, T. B.; Zhulina, Y. B. *Polymer* **1989**, *30*, 170.
(18) Zhulina, E. B.; Adam, M.; LaRue, I.; Sheiko, S. S.; Rubinstein, M. *Macromolecules* **2005**, *38*, 5330.
(19) Jada, A.; Hurtrez, G.; Siffert, B.; Riess, G. *Macromol. Chem. Phys.* **1996**, *197*, 3697.
(20) Won, You-Yeon.; Davis, H.; Ted, Bates.; Frank, S. *Macromolecules* **2003**, *36*, 953.
(21) Abbas, S.; Li, Z.; Hassan, H.; Lodge, T. P. *Macromolecules* **2007**, *40*, 4048.
(22) Honda, C.; Abe, Y.; Nose, T. *Macromolecules* **1996**, *29*, 6778.
(23) Honda, C.; Yuki, H.; Hirunuma, R.; Nose, T. *Macromolecules* **1994**, *27*, 7660.
(24) Dormidontova, E. E. *Macromolecules* **1999**, *32*, 7630.
(25) Pépin, M. P.; Whitmore, M. D. *Macromolecules* **2000**, *33*, 8644.
(26) Haliloluv, T.; Bahar, I.; Erman, B.; Mattice, W. L. *Macromolecules* **1996**, *29*, 4764.
(27) Hadjichristidis, N.; Iatrou, H.; Pispas, S.; Pitsikalis, M. *J. Polym. Sci., Part A: Polym. Chem.* **2000**, *38*, 3211.
(28) LaRue, I.; Adam, M.; da Silva, M.; Sheiko, S. S.; Rubinstein, M. *Macromolecules.* **2004**, *37*, 5002.
(29) Guinier, A.; Fournet, G. *Small-Angle Scattering of X-rays*; John Wiley and Sons: New York, 1955
(30) Press, W. H.; et al. *Numerical Recipes in C, The Art of Scientific Computing*; Plenum Press: NewYork, 1988.
(31) Khougaz, K.; Gao, Z.; Eisenberg, A. *Macromolecules* **1994**, *27*, 6341.
(32) Gao, Z.; Eisenberg, A. *Macromolecules* **1993**, *26*, 7353.
(33) Rubinstein, M.; Colby, R. H. *Polymer Physics*; Oxford University Press: Oxford, UK, 2003.
(34) Lairez, D.; Adam, M.; Carton, J. P.; Raspaud, E. *Macromolecules* **1997**, *30*, 6798.
(35) Below the glass transition temperature of polystyrene (20−100 °C), one measures the linear expansion coefficient $\alpha \simeq 0.7 \times 10^{-4}$ K^{-1}, while above the T_g (100−200 °C), one typically measures a higher coefficient of $\alpha \simeq 6 \times 10^{-4}$ K^{-1}.
(36) Kambour, R. P.; Gruner, C. L.; Romagosa, E. E. *J. Polym. Sci.* **1973**, *11*, 1879.
(37) Krenz, H. G.; Kramer, E. J.; Ast, D. G. *J. Mater. Sci.* **1976**, *11*, 2211.
(38) Earl, B. L.; Loneragan, R. J.; Johns, J. H. T.; Crook, M. *Polym. Eng. Sci.* **1973**, *13*, 390.
(39) Outer, P.; Carr, C. I.; Zimm, B. H. *J. Chem. Phys.* **1950**, *18*, 830.

MA800403R